Smart Structures and Systems, *Vol. 28, No. 2 (2021) 213-228*
https://doi.org/10.12989/sss.2021.28.2.213

Influence of pier height on the effectiveness of seismic isolation of friction pendulum bearing for single-track railway bridges

Weikun He [1,2a], Lizhong Jiang [3,4b], Biao Wei*[3,4] and Zhenwei Wang [5c]

[1] *Key Laboratory for Damage Diagnosis of Engineering Structures of Hunan Province, Hunan University, Changsha 410082, China*
[2] *College of Civil Engineering, Hunan University, Changsha 410082, Hunan, China*
[3] *School of Civil Engineering, Central South University, 22 Shaoshan South Road, Changsha 410075, China*
[4] *National Engineering Laboratory for High Speed Railway Construction, 22 Shaoshan South Road, Changsha 410075, China*
[5] *Zhejiang Scientific Research Institute of Transport, 188 Gangyang Street, Hangzhou 311305, China*

(*Received May 25, 2020, Revised May 18, 2021, Accepted May 26, 2021*)

Abstract. Friction pendulum bearing (FPB) in bridges with different pier heights has various degrees of effectiveness of seismic isolation. To determine the applicability of FPB under different bridge pier height conditions, this paper focuses on the simply supported girder railway bridges that have three types of piers: solid piers with uniform cross-section, solid piers with non-uniform cross-section, and hollow piers with non-uniform cross-section. All of these bridges are first installed with FPB (isolation bearing) and later with non-isolation bearing, modeled by using OpenSEES finite element software. A shake table test is used to verify the related models. Based on nonlinear dynamic time history analysis, the seismic responses of isolated and non-isolated bridges are compared, and their corresponding seismic isolation ratios are calculated. Further, this paper introduces a fuzzy comprehensive evaluation method to determine the seismic isolation effect of FPB on bridges with different pier heights, by weighing and balancing the isolation ratios of different seismic responses of bridges. The results show that the transverse seismic isolation ratios of FPB are generally larger than the longitudinal seismic isolation ratios. In addition, FPB has poorer seismic isolation effect on tall piers compared with short piers.

Keywords: friction pendulum bearing (FPB); fuzzy logic control (FLC); pier height; seismic isolation ratio; shake table test; single-track railway

1. Introduction

Bridges form a major part of high speed railway lines in China, which is the highest in the world in terms of both proportion and quantity; the average bridge occupation ratio in lines is greater than 50% (He *et al*. 2017, Li *et al*. 2019, Wei *et al*. 2019). As China locates between the circum-Indian and the circum-Pacific seismic belts, and all 23 Chinese seismic zones are subject to violent earthquake, earthquake is one of the major causes of damage to Chinese railway bridges (Lin and Xiong 2011). A large number of bridges have suffered severe damage due to earthquakes (Saiidi *et al*. 2014). For instance, 4,840 of a total of 18,358 bridges in Sichuan Province of China were totally or partially damaged during the 2008 Wenchuan Earthquake (Lin *et al*. 2010). Earthquake may give rise to strong vibrations of bridges, causing structural damage and affecting the safe running of trains (Xia *et al*. 2006). In addition, the seismic damage of bridge structure may also result in indirect social and economic losses, related to inhibited efficiency of railway emergency rescue, increased travel time of transportation network, etc. (Padgett *et al*. 2010). These facts highlight the importance of research on seismic isolation of railway bridges in China.

There are several solutions to the problem of seismic bridge damage (e.g., setting isolation bearings and energy dissipation restrainer to reduce seismic strength demand of bridge structures or prestressing the reinforcing tendons to minimize expected damage). Nevertheless, existing bridges in many countries are still built by traditional aseismic design method (Jara *et al*. 2014), which is normally implemented at the expense of microscopic damage to bridge pier (Usami and Kumar 1998, Chen and Jiang 2011, Roy *et al*. 2017). This results in bridge accumulates damage subjected to multiple ground motions, ultimately leading to the bearing capacity of bridge being exceeded, and in some cases, eventual collapse (Ghosh *et al*. 2015). Consequently, it is essential to evaluate the seismic capacity of existing structure systems and search for more effective alternative seismic technologies.

Currently, many scholars suggest that the application of seismic isolation bearing (e.g., laminated rubber bearing, lead rubber bearing etc.) is an effective mean to improve the seismic performance of bridge structures in the seismic design and reinforcement (Han *et al*. 2009, Pan *et al*. 2012, Schanack *et al*. 2012). However, rather than traditional and widely used elastomeric isolation bearings, another type of seismic isolation bearing, the friction pendulum bearing

*Corresponding author, Professor,
E-mail: weibiao@csu.edu.cn
[a] Assistant Professor, E-mail: 15173169596@163.com
[b] Professor, E-mail: lzhjiang@csu.edu.cn
[c] Graduate Research Assistant, E-mail: 59761872@qq.com

Copyright © 2021 Techno-Press, Ltd.

ISSN: 1738-1584 (Print), 1738-1991 (Online)

(FPB), has drawn many scholars' attention. Not only does the FPB have a relatively full parallelogram hysteresis loop, but it can also automatically bring the superstructure back to its initial center position formed by the rise of the superstructure along the spherical sliding surface of the bearing (Briseghella *et al*. 2013). Considerable research to optimize the isolation technology of FPB has led to its greater acceptance and application in the seismic design of bridges. Eröz and Desroches (2008) put forward that for multi-span continuous (MSC) and multi-span simply supported (MSSS) steel girder bridges, which are two of the most common bridge types found in the Central and Southeastern US (CSUS) inventory, the steel fixed and rocker bearings installed in these bridges were easily damaged during earthquakes. They suggested that the seismic performance of these bridges would be improved dramatically by using FPBs instead of existing steel bearings. Tsopelas *et al*. (1996) and Oh and Kim (1998) conducted the experimental comparative study of FPB-isolated and non-isolated bridge, which demonstrated that the seismic capacity of FPB-isolated bridge has been substantially improved, compared with that of non-isolated bridge. Kumar *et al*. (2015) proposed the parametric expressions to reflect the interactions of the coefficient of friction, sliding velocity, axial pressure and temperature They also pointed out that the maximum displacement of the isolation system and floor spectral demands are most affected by the frictional heating under high static axial pressure based on the nonlinear time-history analysis.

Based on the single friction pendulum bearing (FPB), first proposed by Zayas *et al*. (1990), Tsai *et al*. (2003) invented a different base isolator called the multiple friction pendulum system (MFPS), whose displacement capacity is twice that of the single FPB, when these two bearings have the same arrangement for plane dimensions. Furthermore, Fenz and Constantinou (2006) described the behavior of the double concave friction pendulum (DCFP) bearing, which is an adaptation of the single FPB. The DCFP bearing was designed to accommodate larger displacements compared to the single FPB. Also, it would provide flexibility for the designer in that they can set different frictional coefficient and curvature radius for the two sliding surfaces of the DCFP bearing. Although the isolation mechanism of FPB has been fully understood, the whole seismic isolation effect of a seismically isolated bridge (SIB) installed with FPB has been rarely studied. Particularly, a SIB with relatively taller piers is more flexible and has a larger vibration period, which can reduce the transmission of seismic force to the superstructure. Meanwhile, the greater flexibility of piers causes smaller isolator displacement and thus, poorer seismic isolation effect (Eröz and DesRoches 2013). Therefore, it is critical to determine the impact of pier height on a SIB isolated by FPB.

A few studies have been conducted to analyze the seismic isolation effect of isolation bearings on bridges with different pier heights. Mitoulis (2012) performed the dynamic response spectrum analysis on a benchmark bridge with precast I-beams to illustrate the inefficacy of seismic isolation in tall bridge piers. He found that as pier height increases from 5 m to 35 m, the contribution ratio of the isolation bearing displacement to the total seismic displacement of the deck drops from above 90% to below 30%. Karim and Yamazaki (2007) constructed the fragility curves of highway bridges subjected to 250 selected earthquake records. They observed that the level of damage probability for isolated bridges increases as pier height increases. The above-mentioned researches demonstrated that FPB is not a satisfactory solution for seismic isolation when applied in bridges with relatively taller piers, while there are no complete statistics and systematic analyses as yet on the seismic isolation effect of FPB for railway simply supported girder bridges with different pier heights. Therefore, there is urgent need of further research to resolve this problem.

This paper first establishes the dynamic analysis bridge models with different pier heights (4–60 m) for Chinese 32 m simply supported T-shaped girder bridge on single-track railway by utilizing OpenSEES (Open System for Earthquake Engineering Simulation) software; each bridge finite element model (FEM) with varying pier height, adopts two types of bearings (FPB and non-isolation bearing), respectively. Secondly, the reasonability of FEM is validated by the shake table test. Thirdly, based on the nonlinear time-history analysis of both isolated and non-isolated bridge FEMs with different pier heights, their seismic responses are obtained, and meanwhile, the corresponding isolation ratios of FPB are presented. Finally, by adopting the fuzzy logic control (FLC) method, the influence of pier height on the seismic isolation ratios of FPB are quantitatively and comprehensively studied.

2. Finite element model

2.1 Bridge profile

The bridge prototype in this paper is typical Chinese reinforced concrete simply supported girder bridge on single-track railway. Its superstructure is 32.6 m long and 2.7 m tall; it is composed of two prefabricated T-shape beams, connected as a whole by the cast-in-place concrete and the transverse prestressing tendon of bridge deck slabs and diaphragm plates (Fig. 1). The subordinate phase dead load and live load are borne by all beams jointly. The total mass of the main girder is 628.24 t, including the self-mass 297.6 t of girder and other masses 10.126 t/m.

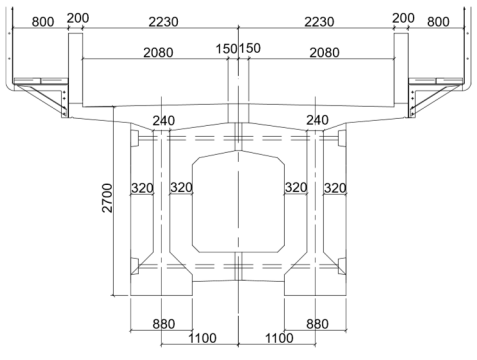

Fig. 1 Dimension of the cross-section of T-shaped beam bridge (unit: mm)

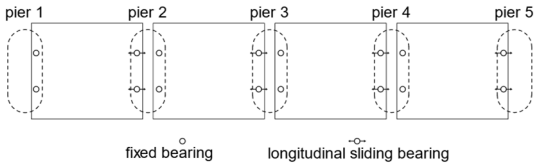

Fig. 2 Bearing arrangement of the simply supported girder bridge for single-track railway

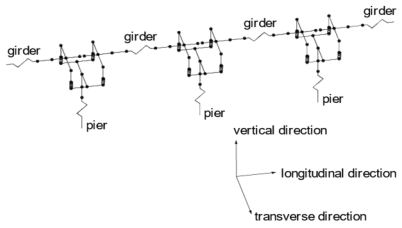

Fig. 3 Local schematic diagram of the bridge models

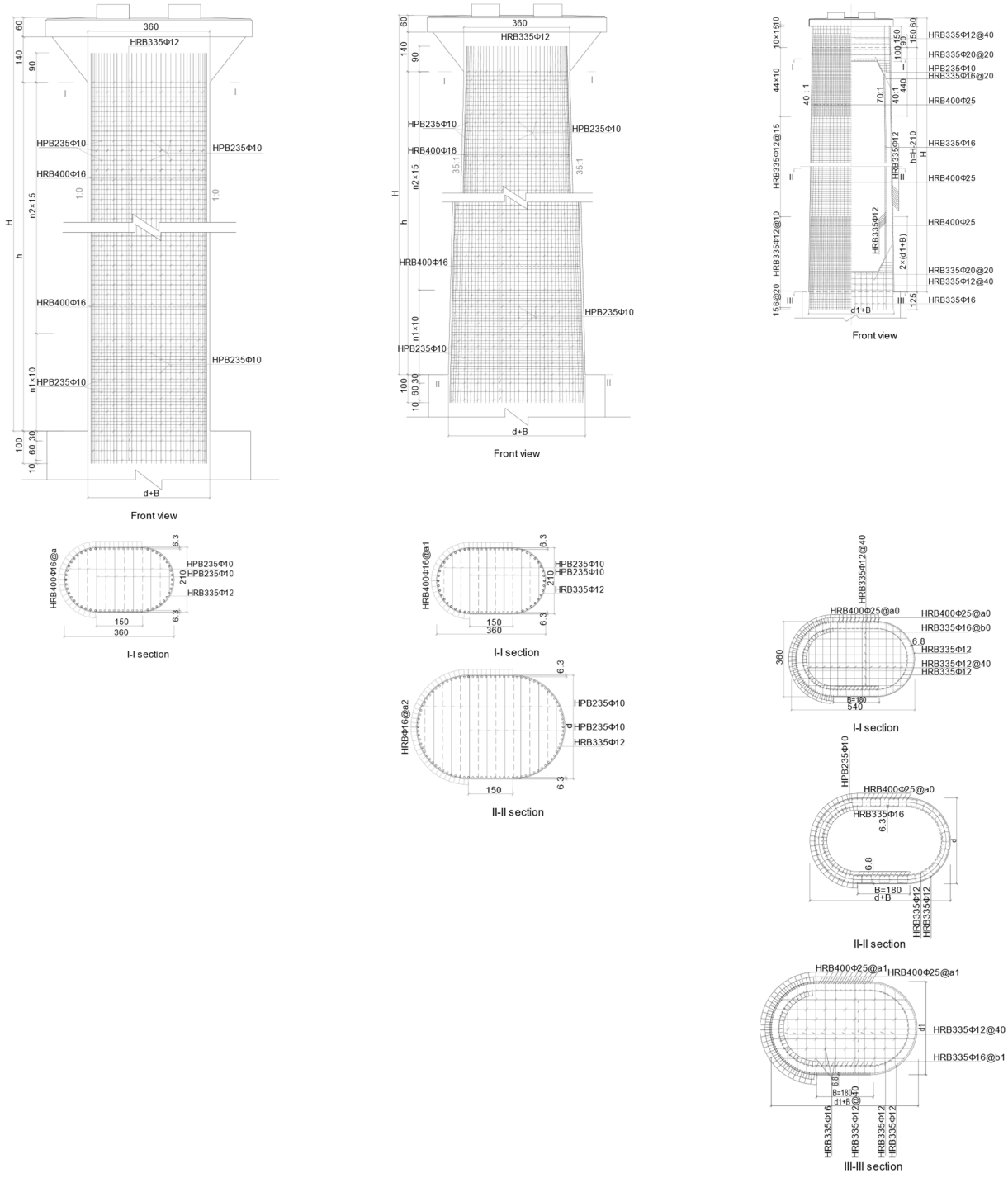

(a) Solid piers with uniform cross-section

(b) Solid piers with non-uniform cross-section

(c) Hollow piers with non-uniform cross-section

Fig. 4 Three types of piers of simply supported girder bridges

The construction of bridge substructure uses single round-ended column pier, supported by pile group foundations. In addition, the type of concrete used for the superstructure and substructure is C55 and C35, respectively, and both of them are reinforced by HPB235, HRB335 and HRB400 steel bars.

This paper sets the FPB, between the main girder and pier. As to evaluate the seismic isolation efficiency of FPB, the non-isolation bearings, i.e., spherical steel bearing, is set as the comparison case. These two types of bearings are placed on the bridge in accordance with the structural form for simply supported girder bridge (Fig. 2), taking into account the effects of shrinkage and creep of concrete and temperature on the free deformation of beams.

Based on the finite element software OpenSEES, a series of bridge models of 4-span simply supported girder bridges, are established under isolated and non-isolated conditions, respectively. All these bridge models vary in pier height. Their local schematic diagram is shown in Fig. 3.

The model of the main girder is represented by the linearly elastic space beam elements. This is because, on the one hand, it is necessary for the superstructure to maintain the elastic state in earthquakes in the seismic design of bridges; on the other hand, no significant damage of main girder of bridges was found in earthquakes according to a large number of actual surveys of seismic damage to bridges (Wei *et al*. 2018, Hu *et al*. 2019).

The model of the pier takes into account the difference between concrete and reinforcement in their nonlinear dynamic characteristics. At the same time, the bottom of the pier is simulated by the fixed constraint and does not account for the interaction effect of structure, pile and soil. Moreover, the total mass of bridge structure itself, railway ballast and other ancillary facilities is evenly distributed to all the nodes of joint elements.

2.2 Piers with different heights

For single-track railway bridges in China, three types of piers have been adopted: solid piers with uniform cross-section, solid piers with non-uniform cross-section, and hollow piers with non-uniform cross-section; corresponding to three ranges of pier height: 4–8 m, 8–25 m and 25–60 m, shown in Fig. 4.

For solid piers with uniform cross-section, the cross-sections of the pier top and pier bottom are the same (Fig. 4(a) and Table 1). For solid piers with non-uniform cross-section, their exterior contour widens from top to bottom with the slope ratio of 35:1 (Fig. 4(b) and Table 2). For hollow piers with non-uniform cross-section, their exterior and interior contours widen from top to bottom with the slope ratio of 40:1 and 70:1, respectively. In addition, for hollow piers, the diameter of longitudinal reinforcements of inner and outer ring of the pier cross-section is 16 mm and 25 mm, respectively (Fig. 4(c) and Table 3).

In this paper, these bridge piers are simulated by nonlinear fiber beam-column elements in OpenSEES software, because not only can they reflect the characteristics of the nonlinearity of different sections and the distribution of reinforcing bars, but also, they have the

Table 1 Dimensions of solid piers with uniform cross-section

H (m)	d (cm)	d+B (cm)	a (cm)	n_1	n_2
4	210	360	14.84	20	0
5	210	360	14.84	30	0
6	210	360	14.84	31	6
7	210	360	14.84	29	14
8	210	360	14.84	30	20

Table 2 Dimensions of solid piers with non-uniform cross-section

H (m)	d (cm)	d+B (cm)	a_1 (cm)	a_2 (cm)	n_1	n_2
9	250	400	13.15	14.94	31	26
10	256	406	12.96	14.98	29	34
11	262	411	12.78	15.02	30	40
12	267	417	12.43	14.86	31	46
13	273	423	12.27	14.9	29	54
14	279	429	10.46	12.9	30	60
15	284	434	11.95	14.98	31	66
16	290	440	11.65	14.83	29	74
17	296	446	11.5	14.87	30	80
18	301	451	11.36	14.91	31	86
19	307	457	11.22	14.94	29	94
20	313	463	11.09	14.98	30	100
21	319	469	10.83	14.84	31	106
22	324	474	10.7	14.87	32	112
23	330	480	10.58	14.91	33	118
24	336	486	10.46	14.94	34	124
25	341	491	10.34	14.98	35	130

Table 3 Dimensions of hollow piers with non-uniform cross-section

H (m)	d (cm)	d+B (cm)	a_1 (cm)	a_2 (cm)	n_1	n_2
30	500	680	15.7	20.5	14.2	17.0
31	505	685	15.7	20.7	14.2	17.1
32	510	690	15.7	20.9	14.2	17.1
33	515	695	15.7	21.0	14.2	17.3
34	520	700	15.7	21.2	14.2	17.4
35	525	705	15.7	21.4	14.2	17.5
36	530	710	15.4	21.1	13.9	17.2
37	535	715	15.4	21.3	13.9	17.3
38	540	720	15.4	21.4	13.9	17.4
39	545	725	15.4	21.6	13.9	17.5
40	547	727	15.4	21.7	13.9	17.5

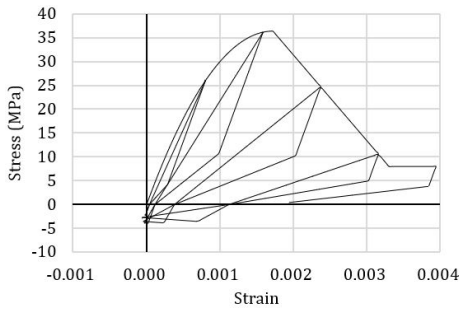

Fig. 5 Stress-strain curve of the concrete in piers

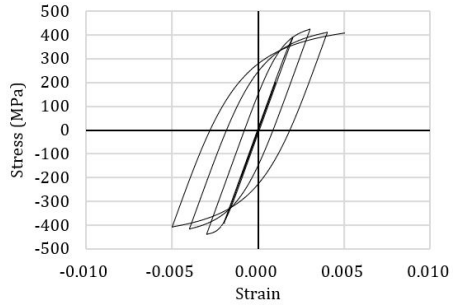

Fig. 6 Stress-strain curve of the main reinforcement in piers

merits of high computational efficiency and accuracy (Mazzoni *et al*. 2006, He *et al*. 2016). The concrete part of the pier section is subdivided into a certain number of discrete elements, each of whose mechanical properties is indicated by the stress-strain relationship of concrete (Fig. 5), while the reinforcement part of the pier section is simulated by the fiber element with identical sectional area, assigned with the stress-strain relationship of reinforcing bars (Fig. 6). Furthermore, the height range of piers of our research is expanded to 4–60 m so the effect of pier height on the isolation efficiency of FPB can be studied in far more detail.

The division of height range for three types piers of bridge FEMs is as follows:

(1) For solid piers with uniform cross-section, nine bridge FEMs are established at the interval of 2 m for pier height ranging from 4 m to 20 m.
(2) For solid piers with non-uniform cross-section, five bridge FEMs are established at the interval of 4 m for pier height ranging from 9 m to 25 m.
(3) For hollow piers with non-uniform cross-section whose height is not more than 40 m, six bridge FEMs are established at the interval of 3 m for pier height ranging from 25 m to 40 m. In addition, for hollow piers whose height is not less than 40 m, their cross-section areas are expanded on the basis of Fig. 4(c), and subsequently, six corresponding bridge FEMs are established at the interval of 4 m for pier height ranging from 40 m to 60 m.

Fig. 5 depicts the stress-strain curve of concrete for the bridge models. Based on OpenSEES software, the material Concrete 01 in this software is adopted to build the constitutive relationship of the core and cover concretes of piers, without considering the tension bearing capacity of concrete, which means that the stress and stiffness of concrete can be assumed to be zero when the compressive strain under seismic loads is less than the residual plastic strain. The material Steel 02 is used to simulate the main reinforcement in piers, and its elastoplastic constitutive relationship approximates to smooth curve (Fig. 6).

2.3 Friction pendulum bearing (FPB) and non-isolated bearing

Different types of bearings are simulated by different connecting elements, which can reflect their corresponding dynamic characteristics. This paper selects two types of bearings, FPB and non-isolation bearing (i.e., double spherical seismic isolation bearing (DSSIB) and spherical steel bearing) to compare their seismic responses and subsequently obtain the seismic isolation ratios of FPB for bridges with different pier heights.

(1) FPB

The DSSIB, being one type of FPB, is composed of one flat friction coupling and two concave friction couplings (Fig. 7).

This paper only considers the seismic responses of the isolated system under strong earthquake loads when there are no shear pins of the bearing (shown in Fig. 7). Shear pins are used in the normal working condition of DSSIB as the inhibiting device that limit the horizontal displacement of the bearing. In strong earthquakes, all shear pins get cut off when the horizontal seismic force is larger than the ultimate bearing capacity of shear pins. After these inhibiting devices are released, the seismic isolation and energy dissipation mechanism of the isolated system is implemented based on the relative slide motion between the concave Teflon sliding plate and concave stainless-steel sliding plate.

The modeling of DSSIB is divided into two parts. On the one hand, the plane motion between the top plate and upper plate of DSSIB is modeled by the flat slider bearing element based on OpenSEES software. On the other hand, the pendulum movements on the upper and bottom concave sliding surfaces of DSSIB can be considered to be equivalent to the motion of the double concave friction pendulum (DCFP) bearing (Khoshnoudian and Hemmati

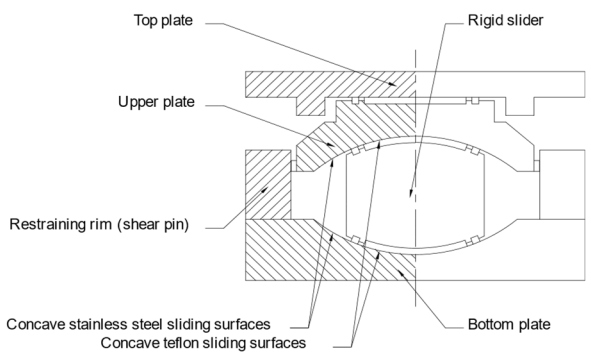

Fig. 7 Schematic of the DSSIB

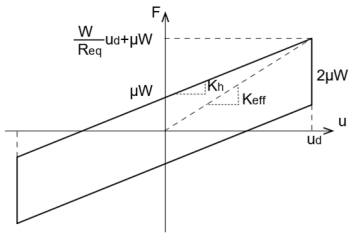

Fig. 8 Hysteresis curve

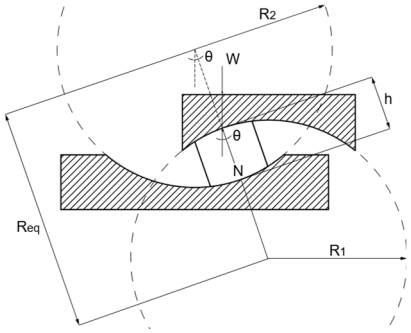

Fig. 9 Cross section of concave sliding surfaces

2014). It is modeled by a combination of two single friction pendulum bearing (FPB) elements in OpenSEES, one of which is upright and the other is upside-down.

The nonlinear behavior of the bearing is described by the bilinear hysteretic model (Fig. 8) (Ponzo *et al*. 2015). R_{eq} is the equivalent curvature radius, μ is the friction coefficient of the upper and bottom sliding surfaces, and u_d is the seismic tolerable displacement ($R_{eq} = R_1 + R_2 - h = 1.5\ m$, $\mu = 0.03$, and $u_d =$ 100 mm).

W is the vertical load of the bearing. For each span of single-track railway bridge, W is equal to 1/4 of the weight of one main girder ($W = 628.24 \times 10^3 kg \times \frac{1}{4} \times 9.8\ N/kg = 1.54 \times 10^3\ kN$). K_h and K_{eff} are the post-yielding stiffness and effective stiffness of the bearing, expressed as follows

$$K_h = \frac{W}{R_{eq}} = \frac{1.54 \times 10^3\ kN}{1.5\ m} = 1027\ kN/m \quad (1)$$

$$\begin{aligned} K_{eff} &= \frac{W}{R_{eq}} + \mu\frac{W}{u_d} \\ &= \frac{1.54 \times 10^3\ kN}{1.5\ m} + 0.03 \times \frac{1.54 \times 10^3\ kN}{0.1\ m} \\ &= 1489\ kN/m \end{aligned} \quad (2)$$

Furthermore, the rise of the superstructure along the spherical sliding surface of the bearing can form a restoring force, which makes the bearing return to its initial position (Fig. 9). The equation for the horizontal restoring force of the DSSIB is given by Fenz and Constantinou (2006) as follows

$$F = \frac{W}{R_{eq}}u + \mu N\cos\theta\ \mathrm{sgn}(\dot{u}) = \frac{W}{R_{eq}}u + \mu W\ \mathrm{sgn}(\dot{u}) \quad (3)$$

where F is the horizontal restoring force, u is the horizontal displacement of the bearing, N is the normal force acting on the sliding surface, $\dot{u}$ is the speed of the bearing, and $\mathrm{sgn}(\dot{u})$ is the sign function (set to 1 when $\dot{u} > 0$, 0 when $u = 0$, and –1 when $\dot{u} < 0$).

It can be seen from Eq. (3) that the horizontal restoring force of the DSSIB consists of two parts: the horizontal component of the superstructure load, and the friction force.

The restoring period of the bearing is presented by Kim and Yun (2007) as follows

$$T_{combi} = 2\pi\sqrt{\frac{R_{eq}}{g}} = 2 \times 3.14 \times \sqrt{\frac{1.5\ m}{9.8\ m/s^2}} = 2.46\ s \quad (4)$$

In order to simplify calculation, this paper only focuses on the horizontal seismic load while the vertical seismic load and friction coefficient of FPB are assumed to be constant. And the vertical part of the bearing is modeled with linear spring elements with exceedingly large stiffness.

(2) Non-isolation bearing

The non-isolation bearing chosen in this paper is the spherical steel bearing, shown in Fig. 10.

In the FEM numerical analysis, the non-isolation bearing is simulated by the flat slider bearing element, assigned with the ideal elastic-plastic constitutive relationship. Its yield displacement (u_d) is 0.002 m, vertical load of the bearing (W) is $1.55 \times 10^3\ kN$, and friction coefficients (μ) in the sliding direction and fixed direction of the bearing are 0.02 and 0.3, respectively.

Subsequently, the initial stiffness of both sliding direction and fixed direction of the bearing can be calculated as follows

$$K = \mu W/u_d \quad (5)$$

Fig. 11 demonstrates the constitutive relation of the

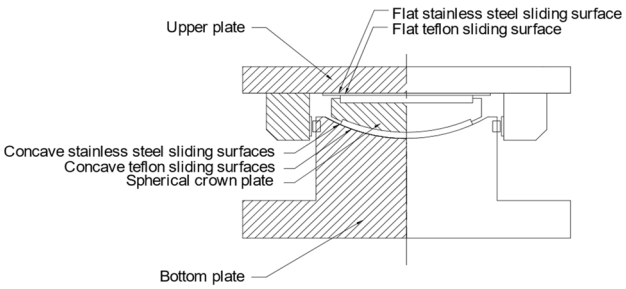

Fig. 10 Schematic of the spherical steel bearing

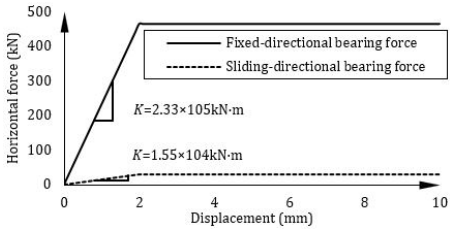

Fig. 11 Constitutive relation of the spherical steel bearing

spherical steel bearing, where $K = 0.02 \times 1.55 \times 10^3\ kN/0.002\ \text{m} = 1.55 \times 10^4\ kN \cdot \text{m}$ in the sliding direction of the bearing, and $K = 0.3 \times 1.55 \times 10^3\ kN/0.002\ \text{m} = 2.33 \times 10^5 kN \cdot \text{m}$ in the fixed direction of the bearing.

3. Ground motion input

The selection of ground motion input in finite element analysis (FEA) is fundamental for carrying out the seismic response analysis of structures, because different structures vary greatly in their seismic responses, depending on the input of earthquake ground motions. In addition, the seismic hazard characteristics and site conditions vary a great deal in different regions. Even if the peak ground accelerations (PGA) of ground motion records from different regions are similar to each other, their seismic response results sometimes have considerable difference. Thus, selecting certain number of ground motion records is necessary in order to study the discreteness of ground motions, and to obtain reasonable conclusions based on statistical analysis. In fact, when 10–20 seismic records are sampled as the ground motion input, it can be used to estimate the seismic hazard as well as the structural safety with a certain accuracy, if PGA, magnitude and duration of selected seismic records are fully considered (Shome and Cornell 1999).

In this paper, 21 man-made earthquake ground motions have been selected as the ground motion input for the models. These man-made waves are generated automatically by using different random phase spectrums to fit the target response spectrum, based on the site conditions of the bridge prototype. The generation of the man-made waves includes the following three steps:

(1) The design response spectrum of 7 seismic sites are chosen according to the seismic safety evaluation at the engineering site. Relevant parameters of ground motion records, including PGA and A_p/V_p (the ratio of peak acceleration to peak velocity of wave), are indicated in Table 4.
(2) The level of exceedance probability of ground motion input is set as 10% probability of exceedance for 50 years; following which, 7 selected design response spectrums are presented according to the level of exceedance probability.
(3) Each design response spectrum for the corresponding site condition is transformed into 3 acceleration time-history curves, whose sampling duration is 24–44 seconds, and time interval of 0.02 seconds.

Table 4 Main parameters of ground motion records

No.	Region	PGA (m/s^{-2})	A_p/V_p (s^{-1})		
			1	2	3
1	Yangjigou	2.27	1.58	4.14	4.38
2	Bailongjiang	1.89	2.31	1.69	4.62
3	Jushuihe	1.99	2.7	3.6	1.58
4	Gaochuanchezhan	2.21	11.56	11.61	11.09
5	Yalong	1.84	8.56	9.99	10.3
6	Jiuzhaigou	1.63	8.28	11.17	8.77
7	Duonuoheihe	1.5	7.67	9.88	10.72

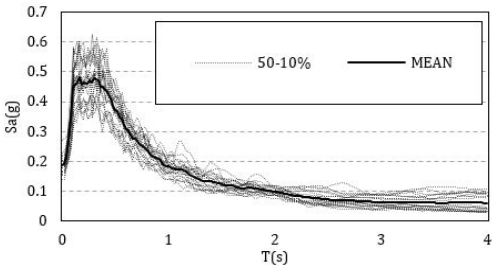

Fig. 12 Response spectrums of earthquake acceleration (damping ratio of 5%)

The response spectrum curves of earthquake acceleration of all 21 man-made earthquake ground motions are shown in Fig. 12, where the dotted lines represent the response spectrums of 21 seismic waves in 7 site conditions, and the solid line expresses the average response spectrum of these 21 seismic waves.

4. Verification of the reasonability of FEM

The shake table test has been performed to verify the rationality and correctness of the simulation method. Two types of simply supported girder bridge models, whose pier

(a) Scaled bridge model with 8 m pier

(b) Scaled bridge model with 25 m pier

Fig. 13 Two experimental bridge models

heights are 8 m and 25 m, respectively, are selected as the test bridge prototypes. Their 1/7-scale experimental bridge models were primarily constructed by Jiang *et al*. (2019), shown in Fig. 13.

This paper chooses one man-made earthquake wave, with exceedance probability of 10% for 50 years (serial 4 in Table 4), as the ground motion input of both the shake table test and the FEA. And the loading direction of this ground motion input for the scaled experimental models and scaled FEMs is unidirectional (longitudinal and transverse).

Based on the results of both the shake table test and the FEA, their seismic responses of bearing displacement and the steel bar strain at the pier bottom are obtained respectively. Figs. 14 and 15 depict the comparisons of time histories of the bearing displacement and the steel bar strain at the pier bottom, respectively. There is little difference

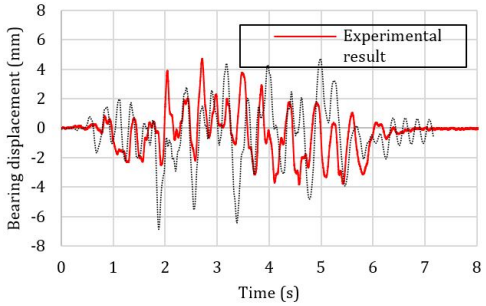

(a) 8 m pier subjected to longitudinal seismic input

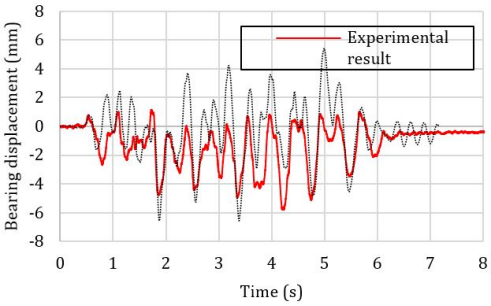

(b) 8 m pier subjected to transverse seismic input

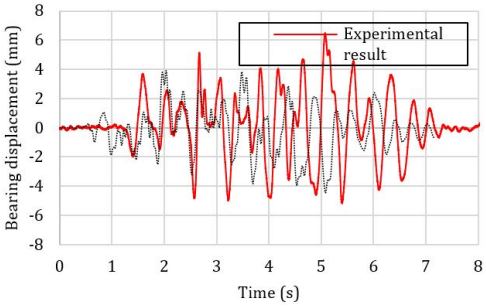

(c) 25 m pier subjected to longitudinal seismic input

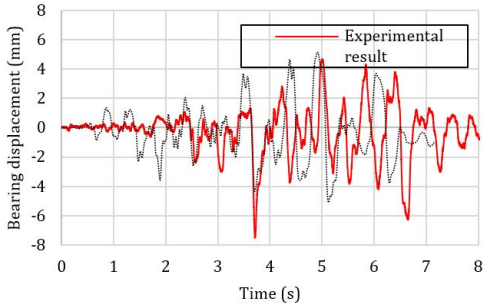

(d) 25 m pier subjected to transverse seismic input

Fig. 14 Time histories of the bearing displacement of scaled bridge models

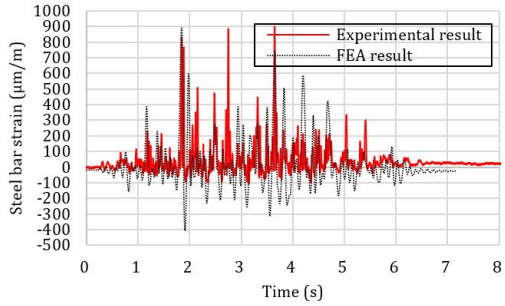

(a) 8 m pier subjected to longitudinal seismic input

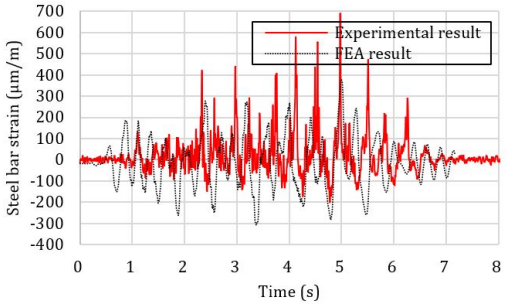

(b) 8 m pier subjected to transverse seismic input

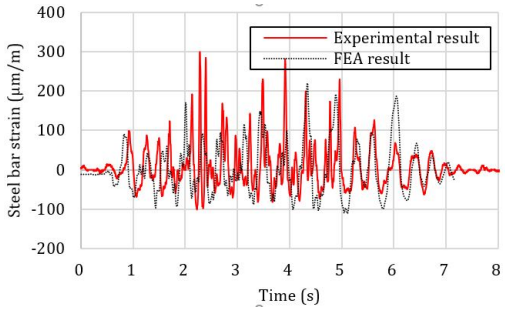

(c) 25 m pier subjected to longitudinal seismic input

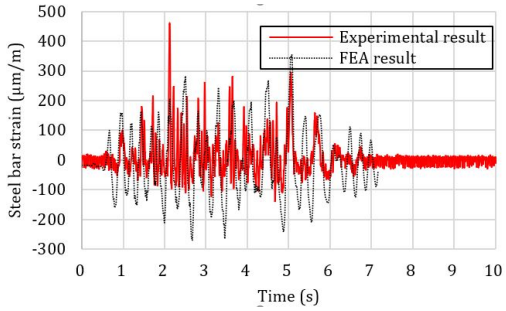

(d) 25 m pier subjected to transverse seismic input

Fig. 15 Time-histories of the steel bar strain at the pier bottom of scaled bridge models

Table 5 Maximum absolute value of experimental and FEA results

Pier height	Bridge direction	Bearing displacement			Steel bar strain at pier bottom		
		Experimental result (mm)	FEA result (mm)	Error (%)	Experimental result (μm/m)	FEA result (μm/m)	Error (%)
8 m	Longitudinal	4.73	4.71	0.44%	899	891	0.89%
	Transverse	5.81	6.58	-13.22%	689	376	45.43%
25 m	Longitudinal	6.48	4.46	31.16%	299	220	26.42%
	Transverse	7.50	5.14	31.44%	461	355	22.99%

between the time-history curves of the experimental and FEA results. In addition, the comparison of maximum absolute values of seismic responses between the experimental models and FEMs are presented in Table 5. The error of maximum absolute values of seismic responses between these two kinds of models reaches its maximum value (45.53%) in the case of the bridge with pier height of 8 m under transverse earthquake ground motion input, when its concrete micro-cracks develop to the greatest extent, resulting in more seismic force being borne by the steel bar (Jiang *et al*. 2019). In other cases, errors are less than 31.44%. Therefore, these errors are acceptable, and the seismic responses of the experimental models are primarily in agreement with the FEMs. These comparison results validate the reasonability of FEMs.

5. Definition of seismic isolation ratio

In order to describe the effect of FPB on energy dissipation, seismic isolation and hazard mitigation for bridges more appropriately, it is necessary to determine the quantitative index to judge the isolation efficiency. This paper mainly focuses on two indexes, the seismic isolation ratio of the displacement at the pier top ($\varnothing_D$) and the seismic isolation ratio of the moment at the pier bottom ($\varnothing_M$). The values of these two indexes are the differences of the maximum displacement at the pier top and the maximum moment at the pier bottom respectively, between non-isolated and isolated bridges, defined as follows

$$\varnothing_D = \frac{D_{max} - D'_{max}}{D_{max}} \tag{6}$$

$$\varnothing_M = \frac{M_{max} - M'_{max}}{M_{max}} \tag{7}$$

where D_{max} and M_{max} are the maximum displacement at the pier top and the maximum moment at the pier bottom of non-isolated bridge, respectively, and D'_{max} and M'_{max} are the maximum displacement at the pier top and the

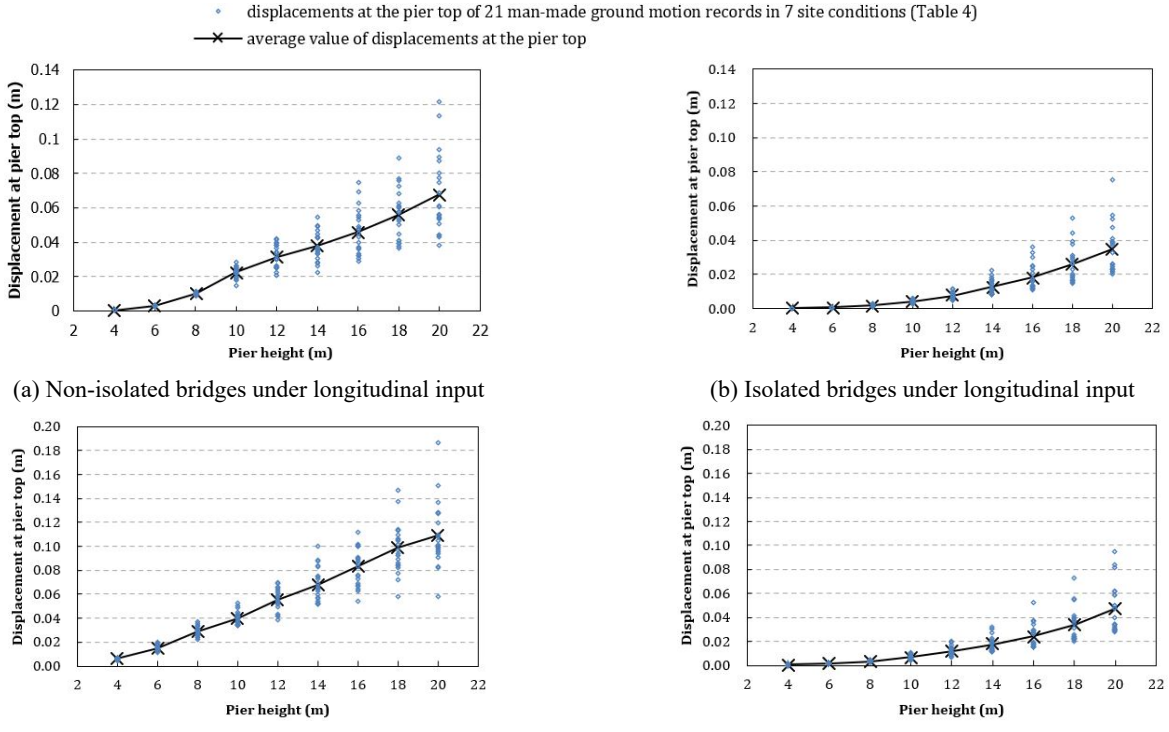

(a) Non-isolated bridges under longitudinal input

(b) Isolated bridges under longitudinal input

(c) Non-isolated bridges under transverse input

(d) Isolated bridges under transverse input

Fig. 16 Influence of pier height on the displacement at the pier top

maximum moment at the pier bottom of isolated bridge, respectively. According to the definitions of seismic isolation ratios (Eqs. (6) and (7)), it is evident that the larger seismic isolation ratio implies a better isolation effect. In addition, this paper only focuses on seismic responses and the corresponding seismic isolation ratio for the central pier of the 4-span simply supported girder bridge models (Pier 3 in Fig. 2).

6. Global effectiveness of seismic isolation of FPB on bridge models

Fig. 16 shows the influence of pier height on the displacement at the pier top for simply supported girder bridges with solid uniform cross-section piers. For longitudinal ground motion input, as the pier height increases from 4 m to 20 m, it results in the increase of the average displacement at the pier top from 0.0006 m to 0.0679 m for non-isolated bridges, and from 0.0002 m to 0.0347 m for isolated bridges (Figs. 16(a) and (b)). Comparably, for transverse ground motion input, there are relatively smaller increases of the displacement at the pier top with the increase of pier height for non-isolated and isolated bridges. In addition, Fig. 16 denotes that the displacement at the pier top of isolated bridges is much smaller than that of non-isolated bridges in the incremental process of pier height in both longitudinal and transverse directions of the bridge. Consequently, FPB can effectively reduce the displacement at the pier top, thus having a beneficial effect on the seismic isolation of the bridge.

Fig. 17 depicts the variation of the seismic isolation ratio of the displacement at the pier top and its standard deviation with pier height. It is demonstrated in Fig. 17(a) that the seismic isolation ratio of the longitudinal displacement at the pier top increases as pier gets higher in the height range of 4–8 m, while decreases in the height range of 8–20 m. This change trend can be explained according to the distribution of the longitudinal natural period of the bridges with different pier heights in the average response spectrum (Fig. 18).

Fig. 18(a) reveals that for non-isolated bridges with pier height of 4–8 m, their longitudinal natural periods are within 0.30–0.39 s, when the corresponding spectral accelerations of the bridges are in the plateau phase of the response spectrum, which means that the period prolongation caused by the increase of pier height results in little increase of the structural response. However, for isolated bridges, their spectral accelerations of the structural natural period are in the rapidly descending stage of the response spectrum, due to the influence of relatively longer natural period of FPB. It means that the increase of pier height leads to the sharp decrease in the structural response. Accordingly, the displacement growth at the pier top of non-isolated bridges is larger than that of isolated bridges (Fig. 18(b)), which is the reason why the seismic isolation ratio of longitudinal displacement at the pier top increases as pier height increases from 4 m to 8 m, shown in Fig.

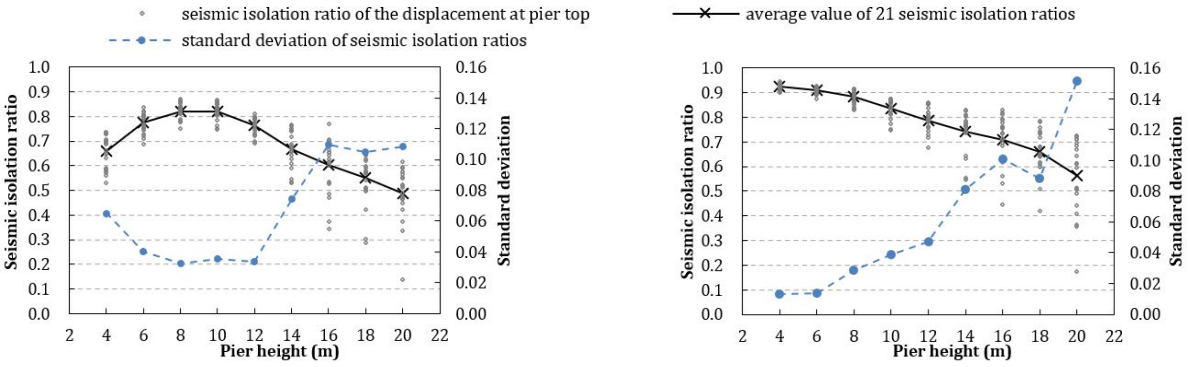

(a) Longitudinal seismic input (b) Transverse seismic input

Fig. 17 Influence of pier height on the seismic isolation ratio of the displacement at the pier top

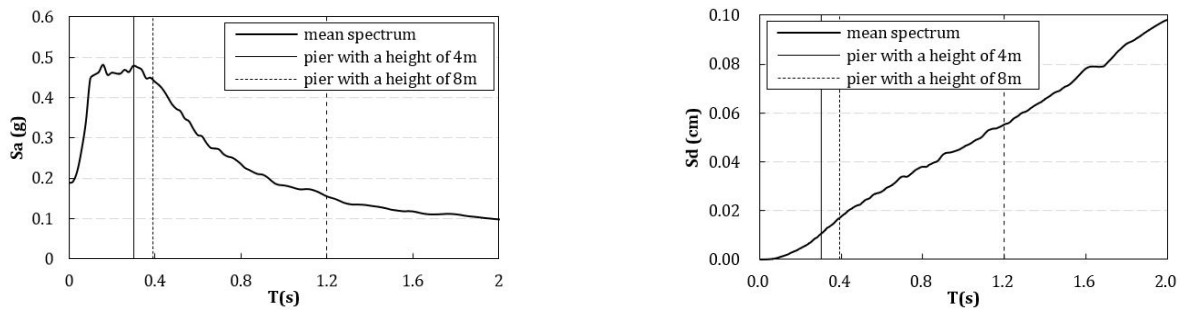

(a) Absolute acceleration response spectrum (b) Relative displacement response spectrum

Fig. 18 Distribution of longitudinal natural period of corresponding bridges with different pier heights on the average seismic response spectrum with 5% damping ratio

17(a). On the contrary, Fig. 17(a) demonstrates a downward trend of seismic isolation ratio of the longitudinal displacement at the pier top as pier gets higher in the height range of 8–20 m. This results from the fact that the spectral acceleration of non-isolated bridges reduces sharply in the response spectrum while the spectral acceleration of isolated bridges decreases slowly when pier height is in the range of 8–20 m (Fig. 18(a)). Hence, the displacement growth at the pier top of non-isolated bridges is smaller than that of isolated bridges (Fig. 16(a) and Fig. 16(b)), which results in the decrease in the seismic isolation ratio after pier height reaches 8 m (Fig. 17(a)).

Fig. 17(b) reveals that the seismic isolation ratio of the transverse displacement at the pier top decreases as pier gets higher, while its decreasing rate increases with pier height, mainly due to the following two factors: (1) For non-isolated bridges under transverse ground motion input, as pier height increases, the displacement at the pier top increases while its rate of increases rarely changes (Fig. 16(c)). (2) For isolated bridges under transverse ground motion input, both the displacement at pier top and its increasing rate become larger as pier gets higher (Fig. 16(d)). As a result, the seismic isolation ratio of the transverse displacement at the pier top decreases significantly (Fig. 17(b)).

Moreover, with the increase of pier height, the standard deviation of the seismic isolation ratio of the longitudinal displacement firstly decreases, and then tends to plateau within the pier height range of 4–12 m, followed by a sharp increase in the standard deviation (from 0.033 to 0.110) within the pier height range of 12–16 m. Ultimately, its standard deviation approximately maintains at 0.11 with the further increase of pier height (Fig. 17(a)). Meanwhile, the discreteness of the transverse seismic isolation ratio to the ground motion input becomes larger with pier height except for 16–18 m height range, and when pier height is 20 m, it reaches its maximum value (0.15) (Fig. 17(b)). Accordingly, for bridges with solid uniform cross-section piers, it can be concluded that the discreteness of the seismic isolation ratio of the displacement with different ground motion inputs is larger for the relatively taller piers.

Figs. 19 and 20 illustrate the influence of pier height on the moment at the pier bottom and its seismic isolation ratio, respectively for bridge models with solid uniform cross-section piers. It is evident that the longitudinal moment at the pier bottom of non-isolated bridges increases linearly as pier height increases from 4 m to 10 m at first; and it then remains around 10000 kN·m after pier height increases above 10 m (Fig. 19(a)). This is because when the moment at the pier bottom is higher than the proportional limit (10000 kN·m), plastic deformation appears at the pier bottom, limiting the growth of the moment due to the stress re-distribution and constitutive relationship of concrete. In comparison to non-isolated bridges, isolated bridges have a consistent growth of the longitudinal moment at the pier bottom with the increase of pier height (Fig. 19(c)). For isolated bridges whose piers are in elastic state all the time, the moment at the pier bottom is determined by both pier height and shear force. As pier gets higher, the moment at the pier bottom increases, because the decreasing rate of shear force is less than the increasing rate of pier height, and vice versa.

Similarly, for non-isolated bridges under transverse seismic input, its moment at the pier bottom firstly increases with pier height of 4–8 m, and it then remains constant around its proportional limit (12500 kN·m) within the pier

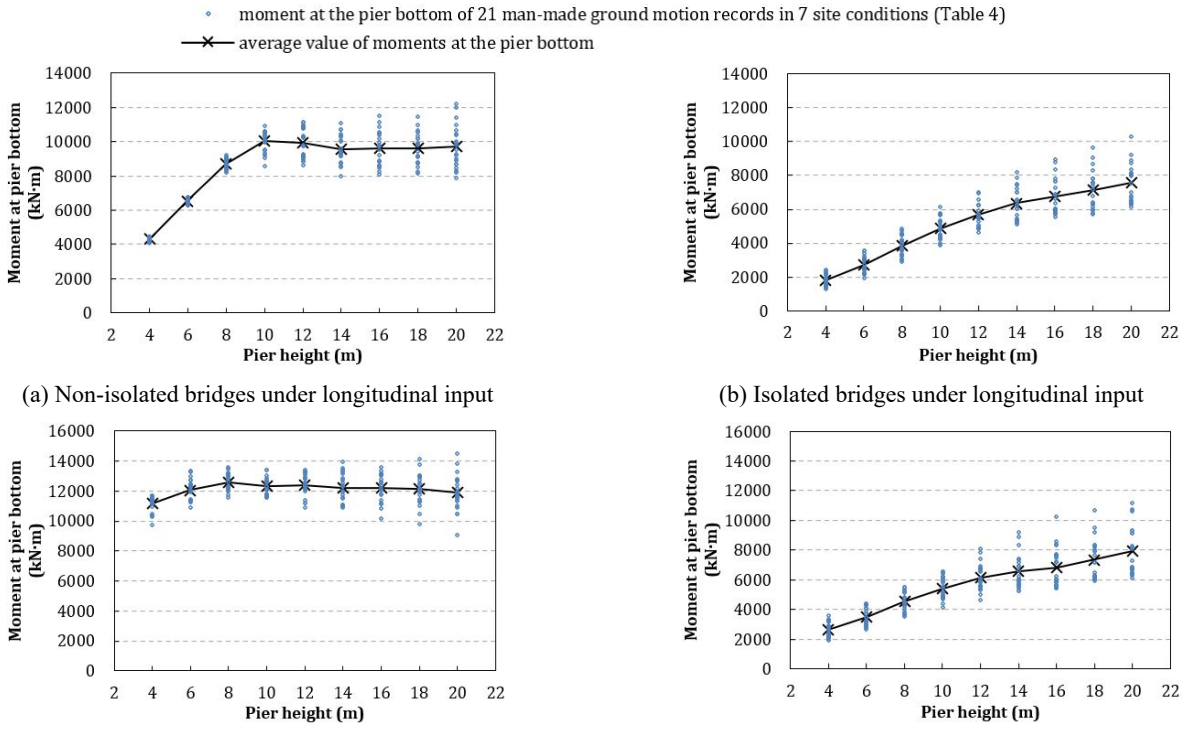

(a) Non-isolated bridges under longitudinal input

(b) Isolated bridges under longitudinal input

(c) Non-isolated bridges under transverse input

(d) Isolated bridges under transverse input

Fig. 19 Influence of pier height on the moment at the pier bottom

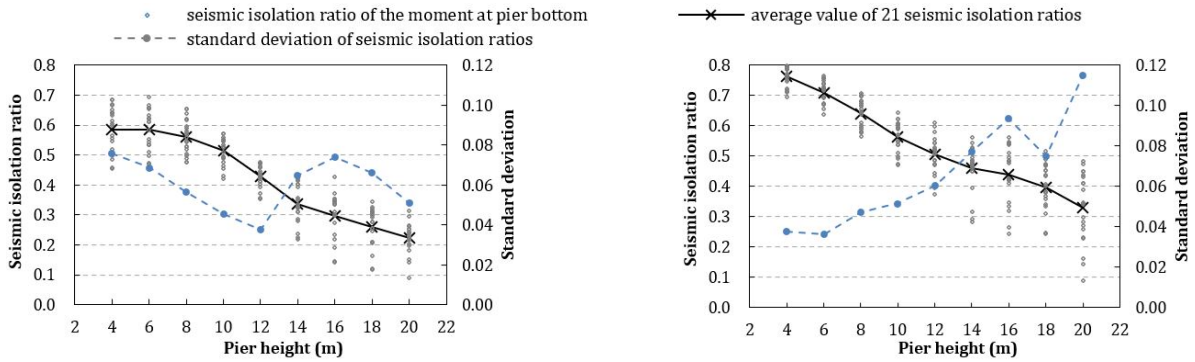

(a) Longitudinal seismic input (b) Transverse seismic input

Fig. 20 Influence of pier height on the seismic isolation ratio of the moment at the pier bottom

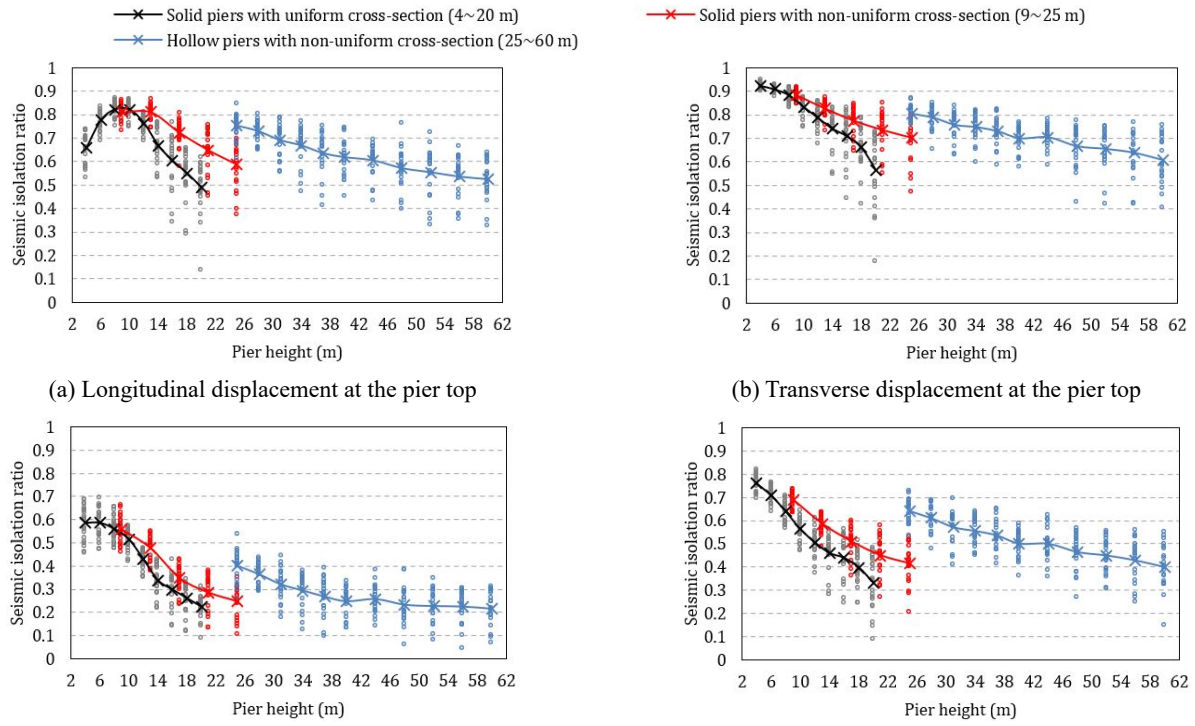

(a) Longitudinal displacement at the pier top (b) Transverse displacement at the pier top

(c) Longitudinal moment at the pier bottom (d) Transverse moment at the pier bottom

Fig. 21 Influence of pier height on the seismic isolation ratio

height range of 8–20 m (Fig. 19(c)). For isolated bridges, their piers are in elastic state all the time, and there is a continuous increase in the transverse moment at the pier bottom with the increase of pier height from 4 m to 12 m and then after that, its growth becomes slightly slower (Fig. 19(d)).

Subsequently, based on the variation tendency of the moment at pier bottom with different pier heights (Fig. 19), it can be concluded that both longitudinal and transverse seismic isolation ratio of moment at the pier bottom decline continuously with the increase of pier height, as depicted in Fig. 20. In addition, for the longitudinal seismic isolation ratio of the moment at the pier bottom, its standard deviation fluctuates in the range of 0.04–0.08 as pier gets higher, and it reaches the minimum value when pier height is 12 m; for the standard deviation of the transverse seismic isolation ratio of moment at the pier bottom, its variation tendency is similar to that of the transverse seismic isolation ratio of the displacement at the pier top (Fig. 17(b)).

The above FEA results are based on the bridge models with solid uniform cross-section piers. The same analysis method is also conducted on the bridge models with solid piers with non-uniform cross-section and hollow piers with non-uniform cross-section. Fig. 21 summarizes the seismic isolation ratios of bridges with the following three types of piers: solid piers with uniform cross-section (4–20 m), solid piers with non-uniform cross-section (9–25 m), hollow piers with non-uniform cross-section (25–60 m).

In Fig. 21, the seismic isolation ratio of the displacement at the pier top is generally greater than that of the moment at pier bottom. In addition, it should be noted that all of the non-isolated bridges with taller piers (25–60

m) remain in elastic state all the time, while the seismic isolation ratios are relatively lower as pier gets higher. It means tall piers can keep elastic even without isolation design, though the seismic isolation effect of FPB on tall piers is not as good as short piers.

7. Evaluation of seismic isolation effects by the fuzzy logic control (FLC)

It is worth mentioning that there is a certain negative correlation between the seismic isolation ratios of the displacement at the pier top ($\varnothing_D$) and the seismic isolation ratio of the moment at the pier bottom ($\varnothing_M$) in Fig. 21, and their maximum values are not reached at the same time. It is difficult to define a screening principle to evaluate the seismic performance of FPB only based on a certain kind of isolation ratio. For instance, engineers cannot figure out whether FPB with $\varnothing_D$ of 50% has good seismic isolation performance. Therefore, this paper uses the method of fuzzy logic control (FLC) to consider the equilibrium between $\varnothing_D$ and $\varnothing_M$, and thus, evaluate the effectiveness of seismic isolation of FPB more comprehensively and synthetically. The concept of fuzzy sets, first proposed by Zadeh in 1965, is used to handle nonlinearity, uncertainty and imprecision in the measurement or system modeling (Choi *et al*. 2004, Lu and Lin 2009, Lin *et al*. 2014).

Fig. 22 presents the architecture of FLC system, which basically consists of three main parts (fuzzification, inference engine and defuzzification): (1) Fuzzification is to map the clear data to the appropriate membership function in order to obtain a series of of fuzzy sets, and each fuzzy set is assigned a linguistic label. (2) Inference engine is used for performing approximate reasoning, based on the rule base about the relationship between fuzzy input and output. (3) Defuzzification is to transform the fuzzy values obtained from the inference engine back into crisp values (Lin *et al*. 2014).

In this paper, FLC system is presented by using the Fuzzy Logic Toolbox (FLT) in MATLAB (Castro *et al*. 2007, 2008), including the following four steps: (1) Two seismic isolation ratios ($\varnothing_D$ and $\varnothing_M$) are set as the crisp (non-fuzzy) input and one new index (comprehensive isolation ratio (χ)) is set as the crisp output. (2) As shown in Fig. 23, a triangular membership function is adopted to assign the relationship between fuzzy and crisp variables. This function is expressed by five fuzzy sets of the seismic isolation performance, namely, Unsatisfactory, Poor, Fair, Good and Excellent. (3) A fuzzy output is obtained by performing approximate reasoning on the fuzzy input, based on the rule base (Table 6). (4) The de-fuzzification process from fuzzy input to crisp value is finally completed by the center of gravity method in FLT (Alcala-Fdez *et al*. 2011).

Fig. 24 demonstrates the relationship between the crisp input ($\varnothing_D$ and $\varnothing_M$) and crisp output (χ). By taking the values of $\varnothing_D$ and $\varnothing_M$ as the crisp input of FLC system, the

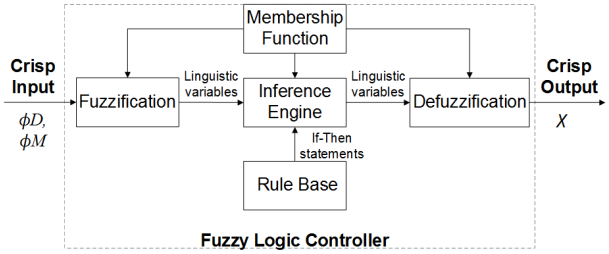

Fig. 22 Architecture of FLC system

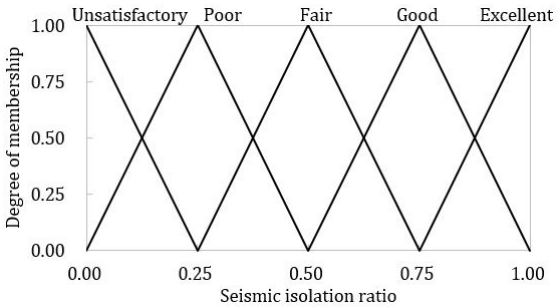

Fig. 23 Membership function of seismic isolation ratio

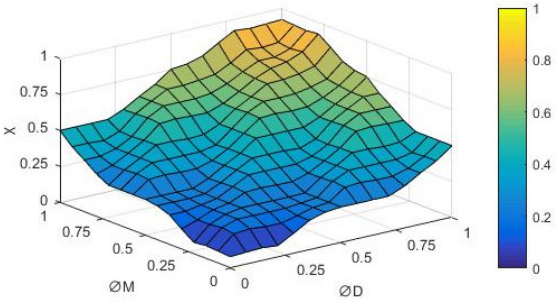

Fig. 24 Input-output relationship of FLC system

Table 6 Rule database of FLC system

Comprehensive isolation ratio (χ)		Seismic isolation ratio of the displacement at the pier top ($\varnothing_D$)				
		Unsatisfactory	Poor	Fair	Good	Excellent
Seismic isolation ratio of the moment at the pier bottom ($\varnothing_M$)	Unsatisfactory	Unsatisfactory	Unsatisfactory	Poor	Poor	Fair
	Poor	Unsatisfactory	Poor	Poor	Fair	Fair
	Fair	Poor	Poor	Fair	Fair	Good
	Good	Poor	Fair	Fair	Good	Excellent
	Excellent	Fair	Fair	Good	Excellent	Excellent

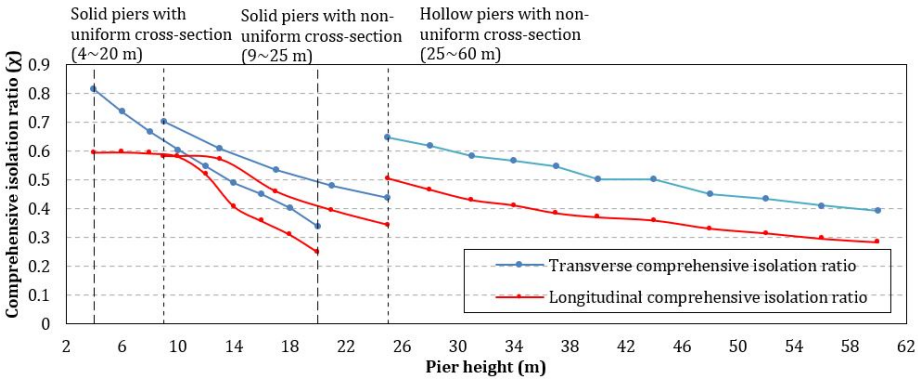

Fig. 25 Influence of pier height on the comprehensive isolation ratio (χ)

corresponding crisp output, i.e., comprehensive isolation ratio (χ) can be calculated by using FLT.

Fig. 25 summarizes the comprehensive isolation ratio (χ) under the conditions of different pier heights. It is evident that the transverse comprehensive isolation ratio is generally larger than the longitudinal one. This mainly because the transverse natural period of the bridge is much less than its longitudinal natural period, and thus, FPB can have a more obvious effect on reducing the structural dynamic response by extending the transverse structural period, compared with the longitudinal one. In addition, χ decreases with the increase of pier height for the bridges with the same pier cross-section type. Therefore, it can be concluded that the seismic isolation effect of FPB is more productive in the case of bridges with relatively shorter piers. Furthermore, χ reaches both its maximum/minimum values (0.595/0.249 in the longitudinal direction of bridge, and 0.815/0.338 in the transverse direction of bridge) within the pier height range of 4–20 m (height range of solid piers with uniform cross-section).

8. Conclusions

This paper takes the simply supported girder bridges on single-track railway in Chinese earthquake region as the study object, and establishes the corresponding FEMs with different pier heights (4–60 m); for each FEM, two types of bearings (FPB and non-isolation bearing) are adopted. The rationality of FEM is validated by the shake table test, which focuses on two types of bridge models with different pier heights (8 m and 25 m). Subsequently, through the nonlinear time-history analysis, which is conducted on both FPB-isolated and non-isolated bridge FEMs, their seismic responses are compared. And the corresponding seismic isolation ratios of FPB under the conditions of different pier heights are calculated. Finally, the seismic isolation ratios of FPB is evaluated comprehensively by the method of FLC. To summarize:

(1) For railway simply supported girder bridges with different pier heights (4–60 m) subjected to longitudinal ground motion input, the seismic isolation ratio of the displacement at the pier top ($\varnothing_D$) grows, while there is no obvious change in the seismic isolation ratio of the moment at the pier bottom ($\varnothing_M$), as pier gets higher in the case of the pier height range of 4–8 m; in other cases, both $\varnothing_D$ and $\varnothing_M$ have a decreasing trend with the increase of pier height.

(2) For railway simply supported girder bridges subjected to transverse ground motion input, both $\varnothing_D$ and $\varnothing_M$ drop as pier gets higher in the height range of 4–60 m.

(3) The discreteness of seismic isolation ratio becomes larger with the increase of pier height, which indicates that FPB has poorer operational reliability in cases of relatively taller piers.

(4) The transverse seismic isolation ratios of FPB are generally larger than the longitudinal seismic isolation ratios. This is mainly because the transverse natural period of the bridge is much less than its longitudinal natural period. Consequently, the transverse isolation effect of FPB on lengthening the natural period of the bridge is better than that of the longitudinal isolation effect.

(5) The FEA results of the seismic isolation ratios of FPB is correct based on the experimental validation, and it can serve as a reference for the selection of the appropriate scope of pier height to maximize the seismic isolation effect of FPB.

(6) The evaluation index (comprehensive isolation ratio (χ)), proposed in this paper, takes into account of the equilibrium of seismic isolation ratios between different seismic responses. The authors further plan to to find a more specific and accurate approach for fuzzy set division of seismic isolation ratios according to the characteristics of seismic isolation demand, and to define the minimum limits of seismic isolation ratios of FPB for designers.

Acknowledgments

This research is jointly supported by the National Natural Science Foundations of China under grant No. 51778635 and 51778630, the Science and Technology Project of Sichuan Province under grant No.

2019YFG0048, the Natural Science Foundations of Hunan Province under grant No. 2019JJ40386, and the Research Program on Key Technology for the Seismic Design of Railway Bridge in Nine Degree Seismic Intensity Zone under grant No. KYY2018059. The above support is greatly appreciated.

References

Alcala-Fdez, J., Alcala, R. and Herrera, F. (2011), "A fuzzy association rule-based classification model for high-dimensional problems with genetic rule selection and lateral tuning", *IEEE T. Fuzzy Syst.*, **19**(5), 857-872. https://doi.org/10.1109/tfuzz.2011.2147794

Briseghella, B., Zordan, T., Liu, T. and Mazzarolo, E. (2013), "Friction pendulum system as a retrofit technique for existing reinforced concrete building", *Struct. Eng. Int.*, **23**(2), 219-224. https://doi.org/10.2749/101686613X13439149157759

Castro, J., Castillo, O. and Melin, P. (2007), "An interval type-2 fuzzy logic toolbox for control applications", *Proceedings of the 2007 IEEE International Fuzzy Systems Conference*, London, UK, July.

Castro, J.R., Castillo, O., Melin, P. and Rodríguez-Díaz, A. (2008), "Building fuzzy inference systems with a new interval type-2 fuzzy logic toolbox", *Trans. Comput Sci.*, **1**, 104-114. https://doi.org/10.1007/978-3-540-79299-4_5

Chen, L.K. and Jiang, L.Z. (2011), "Inelastic displacement spectra for displacement-based seismic design of high-speed railway bridge pier", *Appl. Mech. Mater.*, **121-126**, 892-896. https://doi.org/10.4028/www.scientific.net/AMM.121-126.892

Choi, K.M., Cho, S.W., Jung, H.J. and Lee, I.W. (2004), "Semi-active fuzzy control for seismic response reduction using magnetorheological dampers", *Earthq. Eng. Struct. D.*, **33**(6), 723-736. https://doi.org/10.1002/eqe.372

Eröz, M. and Desroches, R. (2008), "Bridge seismic response as a function of the Friction Pendulum System (FPS) modeling assumptions", *Eng. Struct.*, **30**(11), 3204-3212. https://doi.org/10.1016/j.engstruct.2008.04.032

Eröz, M. and DesRoches, R. (2013), "The influence of design parameters on the response of bridges seismically isolated with the Friction Pendulum System (FPS)", *Eng. Struct.*, **56**, 585-599. https://doi.org/10.1016/j.engstruct.2013.05.020

Fenz, D.M. and Constantinou, M.C. (2006), "Behaviour of the double concave friction pendulum bearing", *Earthq. Eng. Struct. D.*, **35**(11), 1403-1424. https://doi.org/10.1002/eqe.589

Ghosh, J., Padgett, J.E. and Sánchez-Silva, M. (2015), "Seismic damage accumulation in highway bridges in earthquake-prone regions", *Earthq. Spectra.*, **31**(1), 115-135. https://doi.org/0.1193/120812eqs347m

Han, Q., Du, X., Liu, J., Li, Z., Li, L. and Zhao, J. (2009), "Seismic damage of highway bridges during the 2008 Wenchuan earthquake", *Earthq Eng Eng. Vib.*, **8**(2), 263-273. https://doi.org/10.1007/s11803-009-8162-0

He, R., Yang, Y. and Sneed, L.H. (2016), "Post-repair seismic assessment of RC bridges damaged with fractured column bars - A numerical approach", *Eng. Struct.*, **112**, 100-113. https://doi.org/10.1016/j.engstruct.2016.01.007

He, X., Wu, T., Zou, Y., Chen, Y.F., Guo, H. and Yu, Z. (2017), "Recent developments of high-speed railway bridges in China", *Struct. Infrastruct. E.*, **13**(12), 1584-1595. https://doi.org/10.1080/15732479.2017.1304429

Hu, M., Han, Q., Wen, J. and Bai, Y. (2019), "Seismic failure of multi-span simply supported RC slab-on-grider bridge in 2008 Wenchuan earthquake: Case study", *Eng. Fail. Anal.*, **95**, 140-153. https://doi.org/10.1016/j.engfailanal.2018.09.011

Jara, J.M., López, M.G., Jara, M. and Olmos, B.A. (2014), "Rotation and damage index demands for RC medium-length span bridges", *Eng. Struct.*, **74**, 205-217. https://doi.org/10.1016/j.engstruct.2014.05.029

Jiang, L., He, W., Wei, B., Wang, Z. and Li, S. (2019), "The shear pin strength of friction pendulum bearings (FPB) in simply supported railway bridges", *B. Earthq. Eng.*, **17**(11), 6109-6139. https://doi.org/10.1007/s10518-019-00698-x

Karim, K.R. and Yamazaki, F. (2007), "Effect of isolation on fragility curves of highway bridges based on simplified approach", *Soil. Dyn. Earthq. Eng.*, **27**(5), 414-426. https://doi.org/10.1016/j.soildyn.2006.10.006

Khoshnoudian, F. and Hemmati, T.A. (2014), "Impact of structures with double concave friction pendulum bearings on adjacent structures", *P. I. Civil Eng.-Str. B.*, **167**(1), 41-53. https://doi.org/10.1680/stbu.12.00001

Kim, Y.S. and Yun, C.B. (2007), "Seismic response characteristics of bridges using double concave friction pendulum bearings with tri-linear behavior", *Eng. Struct.*, **29**(11), 3082-3093. https://doi.org/10.1016/j.engstruct.2007.02.009

Kumar, M., Whittaker, A.S. amd Constantinou, M.C. (2015), "Characterizing friction in sliding isolation bearings", *Earthq. Eng. Struct. D.*, **44**(9), 1409-1425. https://doi.org/10.1002/eqe.2524

Li, D., Cao, M., Deng, T. and Zhang, S. (2019), "Wavelet packet singular entropy-based method for damage identification in curved continuous girder bridges under seismic excitations", *Sensors*, **19**(19), 4272. https://doi.org/10.3390/s19194272

Lin, S. and Xiong, H. (2011), *Advances in Computer Science, Environment, Ecoinformatics, and Education, Part II: International Conference*, CSEE 2011, Wuhan, China, August, pp. 526-527.

Lin, C.C.J., Hung, H.H., Liu, K.Y. and Chai, J.F. (2010), "Reconnaissance observation on bridge damage caused by the 2008 Wenchuan (China) earthquake", *Earthq. Spectra.*, **26**(4), 1057-1083. https://doi.org/10.1193/1.3479947

Lin, T.-K., Lu, L.-Y. and Chang, H. (2014), "Fuzzy logic control of a stiffness-adaptable seismic isolation system", *Struct. Control Health Monitor.*, **22**(1), 177-195. https://doi.org/10.1002/stc.1667

Lu, L.-Y. and Lin, G.-L. (2009), "Fuzzy friction controllers for semi-active seismic isolation systems", *J Intel. Mater. Syst. Struct.*, **20**(14), 1747-1770. https://doi.org/10.1177/1045389X09343788

Mazzoni, S., McKenna, F., Scott, M.H. and Fenves, G.L. (2006), *OpenSEES command language manual*, Department of Civil Environmental Engineering University of California, Berkeley, CA, USA, pp.134-142.

Mitoulis, S.A. (2012), "The Inefficacy of Seismic Isolation in Bridges with Tall Piers", *Proceedings of the 15th World Conference on Earthquake Engineering*, Lisbon, Portugal, September.

Oh, S.-T. and Kim, Y.S. (1998), "Experimental and analytical investigation of a seismically isolated bridge model with friction pendulum system", *KSCE J. Civil Eng.*, **2**(3), 265-272. https://doi.org/10.1007/BF02830480

Padgett, J.E., Dennemann, K. and Ghosh, J. (2010), "Risk-based seismic life-cycle cost benefit (LCC-B) analysis for bridge retrofit assessment", *Struct. Saf.*, **32**(3), 165-173. https://doi.org/10.1016/j.strusafe.2009.10.003

Pan, P., Ye, L., Shi, W. and Cao, H. (2012), "Engineering practice of seismic isolation and energy dissipation structures in China", *Sci. China Technol. Sci.*, **55**(11), 3036-3046. https://doi.org/10.1007/s11431-012-4922-6

Ponzo, F.C., Cesare, A.D., Leccese, G. and Nigro, D. (2015), "Shaking table tests of a base isolated structure with double concave friction pendulum bearings", *Bull. New Zealand Soc.*

Earthq. Eng., **48**(2), 136-144. https://doi.org/10.5459/bnzsee.48.2.136-144

Roy, A., Bhattacharya, G. and Roy, R. (2017), "Maximum credible damage of RC bridge pier under bi-directional seismic excitation for all incidence angles", *Eng. Struct.*, **152**, 251-273. https://doi.org/10.1016/j.engstruct.2017.09.008

Saiidi, M.S., Vosooghi, A., Choi, H. and Somerville, P. (2014), "Shake table studies and analysis of a two-span RC bridge model subjected to a fault rupture", *J. Bridge Eng.*, **19**(8), A4014003. https://doi.org/10.1061/(ASCE)BE.1943-5592.0000478

Schanack, F., Valdebenito, G. and Alvial, J. (2012), "Seismic Damage to Bridges during the 27 February 2010 Magnitude 8.8 Chile Earthquake", *Earthq. Spectra.*, **28**(1), 301-315. https://doi.org/10.1193/1.3672424

Shome, N. and Cornell, C.A. (1999), "Probabilistic seismic demand analysis of nonlinear structures", Ph.D. Dissertation; Stanford University, Stanford, CA, USA.

Tsai, C.S., Chiang, T.C. and Chen, B.J. (2003), "Seismic behavior of MFPS isolated structure under near-fault sources and strong ground motions with long predominant periods", *Proceedings of the ASME Pressure Vessels and Piping Conference*, Cleveland, OH, USA, July.

Tsopelas, P., Constantinou, M.C., Kim, Y.S. and Okamoto, S. (1996), "Experimental study of FPS system in bridge seismic isolation", *Earthq. Eng. Struct. D.*, **25**(1), 65-78. https://doi.org/10.1016/0148-9062(96)81967-X

Usami, T. and Kumar, S. (1998), "Inelastic seismic design verification method for steel bridge piers using a damage index based hysteretic model", *Eng. Struct.*, **20**(4-6), 472-480. https://doi.org/10.1016/S0141-0296(97)00023-0

Wei, B., Yang, T., Jiang, L. and He, X. (2018), "Effects of uncertain characteristic periods of ground motions on seismic vulnerabilities of a continuous track–bridge system of high-speed railway", *B. Earthq. Eng.*, **16**(9), 3739-3769. https://doi.org/10.1007/s10518-018-0326-8

Wei, B., Li, C., Jia, X., He, X. and Yang, M. (2019), "Effects of shear keys on seismic performance of an isolation system", *Smart Struct. Syst.*, *Int. J.*, **24**(3), 345-360. https://doi.org/10.12989/sss.2019.24.3.345

Xia, H., Han, Y., Zhang, N. and Guo, W. (2006), "Dynamic analysis of train-bridge system subjected to non-uniform seismic excitations", *Earthq. Eng. Struct. D.*, **35**(12), 1563-1579. https://doi.org/10.1002/eqe.594

Zadeh, L.A. (1965), "Fuzzy Sets", *Inf. Control*, **8**(3), 338-353. https://doi.org/10.1016/S0019-9958(65)90241-X

Zayas, V.A., Low, S.S. and Mahin, S.A. (1990), "A simple pendulum technique for achieving seismic isolation", *Earthq. Spectra*, **6**(2), 317-333. https://doi.org/10.1193/1.1585573